fractal and fractional

MDPI

Article

Enhancing Transient Stability in Multi-Machine Power Systems through a Model-Free Fractional-Order Excitation Stabilizer

Arman Fathollahi * and Björn Andresen

Department of Electrical and Computer Engineering, Aarhus University, 8200 Aarhus, Denmark
* Correspondence: arman.f@ece.au.dk

Abstract: The effective operation of model-based control strategies in modern energy systems, characterized by significant complexity, is contingent upon highly accurate large-scale models. However, achieving such precision becomes challenging in complex energy systems rife with uncertainties and disturbances. Controlling different parts of the energy system poses a challenge to achieving optimal power system efficiency, particularly when employing model-based control strategies, thereby adding complexity to current systems. This paper proposes a novel model-independent control approach aimed at augmenting transient stability and voltage regulation performance in multi machine energy systems. The approach involves the introduction of an optimized model-free fractional-order-based excitation system stabilizer for synchronous generators in a multi machine energy system. To overcome the limitations associated with complex system model identification, which add degrees of simplification at defined operating conditions and assume the system model remains fixed despite high uncertainty and numerous disturbances, an optimal model-independent fractional-order-based excitation control strategy is introduced. The efficacy of the proposed approach is validated through comparative numerical analyses using the MATLAB/Simulink environment. These simulations were conducted on a two-area, 12-bus multi-machine power system. Simulation results demonstrate that the presented excitation system stabilizer outperforms conventional controllers in terms of transient and small-signal stability. It also suppresses the low-frequency electromechanical oscillations within the multimachine energy system.

Keywords: power system stabilizer (PSS); model-free control; small-signal stability; fractional-order controller; optimization algorithms; power system; mathematical model

check for updates

Citation: Fathollahi, A.; Andresen, B. Enhancing Transient Stability in Multi-Machine Power Systems through a Model-Free Fractional-Order Excitation Stabilizer. *Fractal Fract.* **2024**, *8*, 419. https://doi.org/10.3390/fractalfract8070419

Academic Editors: Manashita Borah and Christos Volos

Received: 30 April 2024
Revised: 30 June 2024
Accepted: 10 July 2024
Published: 17 July 2024

Copyright: © 2024 by the authors. Licensee MDPI, Basel, Switzerland. This article is an open access article distributed under the terms and conditions of the Creative Commons Attribution (CC BY) license (https://creativecommons.org/licenses/by/4.0/).

1. Introduction

The evolution of electrical power systems has transitioned from local, rudimentary setups to interconnected networks of transmission lines. This new configuration has heralded a new era of complexity. In the modern power system landscapes the challenges of achieving transient and small-signal stability in multi-machine power systems have become increasingly daunting and pose significant hurdles for engineers. This challenge becomes more intense with the integration of renewable energy sources, distributed generation and diverse, unpredictable loads [1,2].

The stability concerns stem from low-frequency electromechanical oscillations. They occur within synchronous generators following different types of disturbances. With frequencies ranging from 0.2 to 3 Hz, these oscillations result from imbalances between mechanical and electrical torques. Commonly referred to as local and inter-area oscillations [3,4]. Such oscillations exert stress on mechanical shafts, diminishing overall operational efficiency and threatening system security and power transmission capabilities [5,6]. During the synchronous operation of generators and loads within a power system at a pre-determined frequency, the difference in the synchronous speed increases the risk of generating transient and small-signal instability. Therefore, swift control action plans in

terms of exciter or turbine controller settings are necessary to maintain synchronous speed despite these deviations.

On the other hand, existing controller configurations and networking conditions can worsen the aforementioned issues, which can, in turn, endanger system stability [7,8]. Of all the problems, high-speed excitation mechanisms are the main ones, as they can deprive the power system of the necessary damping, which is critical for maintaining the stability of the system during a momentary lack of synchronizing torque and for enhancing transient stability. Knowledge about the complicated characteristics of transient and small-signal instabilities in a modern power system is an essential factor in control strategies to maintain the reliability and resilience of the system [9,10].

To address these challenges, Power System Stabilizers (PSSs) in combination with the Automatic Voltage Regulator (AVR) have been integrated into multi-machine power systems to enhance the transient and small-signal stability of the synchronous generators [11,12]. Different types of linear and nonlinear PSSs are proposed in the literature. The literature presents various types of linear and nonlinear supplementary excitation control methods.

In linear control categories, advanced techniques such as linear quadratic gaussian (LQR) methods [13], feedback linearization control [14,15], linear matrix inequality controllers [16,17] and fuzzy logic control strategies [18,19] have been suggested to enhance power system performance. Furthermore, the stabilizers formulated based on linearized power system models have disadvantages. Firstly, linearized models might not depict the nonlinear dynamics of the power system across all operational scenarios effectively. This potentially leads to suboptimal performance. It could also cause instability. Thus, linear controllers might not address disturbances or uncertainties inherent in real-world power systems [20,21]. In addition, linear approaches only ensure proper operation in the vicinity of equivalent points. These points are around which the linearized model of the power system is derived. To address the abovementioned challenges, researchers propose various nonlinear control methodologies, such as adaptive control techniques [22], robust control strategies [23] and nonlinear model predictive control approaches [24]. Sliding mode control (SMC) stands out as a prominent nonlinear and reliable technique for crafting excitation system controllers [25]. In pursuit of enhancing system stability [26] proposes sliding mode control equipping quadratic reduction implemented on single-machine infinite-bus power systems. The second-order sliding mode control (SOSMC) is introduced in [27]. This adaptive technique mitigates low-frequency oscillations effectively and expands the boundaries of conventional SMC.

A comparative analysis in [28] demonstrates the control performance efficiency of the SOSMC over the traditional PSSs in mitigating modeling uncertainties and reduces low-frequency oscillations. These advancements were validated through simulations conducted on IEEE 10-bus and 39-bus systems. Furthermore, a nonlinear backstepping PSS rooted in a fourth-order model of the synchronous machine is presented in [29]. This method enhances the transient stability of the studied power system by suppressing oscillations. The validation of this approach used a power system model featuring three machines. Addressing inherent chattering issues in SMC synergetic control theory emerges as a promising solution. Reference [30] introduces a nonlinear excitation system founded on synergetic control theory, entirely synthesizing the PSS design from a streamlined nonlinear power system model. Furthermore, ref. [31] enhances the performance and stability of power systems by introducing a decentralized synergetic PSS specifically tailored for multi-machine energy systems. A power system oscillation damping controller designed based on model-predictive control and extended state observers is introduced for multi-machine power systems in [24].

The nonlinear control strategies designed for enhancing power system stability and voltage regulation can overcome the limitations of linear based controllers but their effectiveness is still highly dependent on the accurate dynamic models of the power system [32,33]. These detailed models are essential to ensuring that the excitation system stabilizers op-

erate effectively across diverse operating conditions. On the other hand, because of the highly nonlinear and complex nature of modern power systems, coupled with various external disturbances, unknowns and uncertainties, extracting a precise power system model becomes critical and more complex [32].

Particularly in systems with high levels of unmodeled dynamics and uncertainties, model-free controllers (MFCs) show promise as a remedy to the issues of model identification [1]. MFC frameworks provide convincing methods for power system stabilization. They do this without the requirement for detailed model identification. By continuously updating input/output (I/O) data and implementing an observer, MFC systems predict disturbances using the ultra-local model (ULM) [34]. The benefits of ultra-local models in systems with time-varying features, such as power systems, are considerable. ULMs simplify the control procedure by eliminating complicated system dynamics. They convert dynamics into an updateable and controllable structure. Since the real-time updating process enables the controller to adjust to changes and disturbances, ULM guarantees steady performance throughout different operating situations. ULMs avoid the requirement for in-depth parameter identification and system modeling [35,36]. Consequently, their adoption decreases computational calculations resulting in rapid adoption and lower maintenance costs. Intelligent model-independent controllers [37] and ultra-local controllers used in various applications [38] have been developed to address the challenges posed by the complex dynamics of modern power systems. For instance, in [39], a non-singular fast terminal sliding mode controller based on robust model-free techniques was devised to mitigate permanent magnet synchronous motor demagnetization.

Model-free controllers have found applications beyond different electrical systems, such as robots, shipboard power systems (SPSs) and aircraft power distribution networks [40]. Another example is the application of the MFC scheme in microgrids, where a model-independent controller utilizing sliding mode control theory was introduced for a time delay standalone microgrid system [41]. The defined control strategy aimed to optimize power management, balance generation and load requirements. The MFCs exhibit reduced dependency on system dynamics while demonstrating adaptability to changing system parameters. Given the intricate mechanics and unstable nature of modern large-scale power systems deriving accurate mathematical models for such systems poses significant challenges. The characteristics of the MFCs make these controllers suitable for power system stabilization.

In line with the preceding discussion, this paper proposes a novel model-free fractional calculus-based excitation system stabilizer grounded on the ultra-local control concept and fractional-order calculus. The aim is to enhance transient performances and suppress low-frequency electromechanical oscillations in multimachine power systems. To optimize the performance of the suggested stabilizer, a fractional calculus-based particle swarm optimization algorithm is employed within the stabilizer control structure. The proposed practical stabilizer solves the challenges associated with obtaining precise mathematical models for modern multi-machine power systems, particularly in the face of parametric uncertainty and asymptotic stability concerns.

Fractional Calculus (FC) enlarges the domain of classical mathematical theories, especially fractional derivatives and integrals. Contrarily to traditional calculus, fraction orders, on which fractional calculus (FC) is based, are parameter-dependent. Its adaptability has many advantages. First, it provides more accurate descriptions of real-world phenomena when processes exhibit abnormal or memory effects that cannot be sufficiently represented by integer-order models. It is also established that FC reduces control accuracy in control systems, which leads to improved control performance and stability in engineering applications. In addition, it offers new ways to think about and solutions for differential equations and can be particularly useful when traditional methods fail, especially in complex systems [42].

In this paper, an FC-based PSO (FCPSO) algorithm is presented to adjust the parameters of the model-free excitation system stabilizer. By enabling the controller to dynamically

tune its coefficients, this integration improves the controller's robustness and flexibility to changing operating conditions. Finally, this paper incorporates a rigorous and comprehensive numerical analysis, demonstrating the effect of the proposed control framework in a two-area multi-machine power system. The remainder of this work is structured as follows: The modeling of a multi-machine power system with interconnected generators is covered in Section 2. Section 3 provides an illustration of the design of the optimal excitation system stabilizer that is offered. It is based on a combination of a fractional-order calculus framework and an ultra-local idea. The performance of the controller provided has been proven by the simulation results in Section 4. An outline of the conclusions and possible directions for further research is provided in Section 5.

2. Dynamic Model of a Multi-Machine Power System

This section focuses on the modeling of the multi-machine energy system. In this system structure, interconnected generators, lines and transformers serve distinct energy demands of various loads. Figure 1 depicts a two-area, four-machine power system. This system serves as a representative example of a multi-machine energy system [43]. Each generator is treated as an individual subsystem and a decentralized, optimal model-free excitation stabilizer is designed for it. By incorporating certain standard assumptions, we can outline the dynamical model of this m-machine power system, consisting of m interconnected subsystems, as follows [44]:

$$\dot{\delta}_j = \omega_0(\omega_j - 1), \tag{1}$$

$$\dot{\omega}_j = -\frac{1}{2H_j}(P_{ej} - P_{mj}) - \frac{D_j}{2H_j}(\omega_j - 1), \tag{2}$$

$$\dot{E}'_{qj} = -\frac{1}{T'_{d0j}}\left(E'_{qj} + I_{dj}\left(x_{dj} - x'_{dj}\right) - E_{fdj}\right), \tag{3}$$

where $j = 1, 2, 3, \ldots, m$. The following grid-algebraic equations can be employed to characterize the power system's static features:

$$I_{dj} = \sum_{i=1}^{m} E'_{qi}\left(G_{ji}\sin(\delta_j - \delta_i) - B_{ji}\sin(\delta_j - \delta_i)\right), \tag{4}$$

$$I_{qj} = \sum_{i=1}^{m} E'_{qi}\left(B_{ji}\sin(\delta_j - \delta_i) + G_{ji}\sin(\delta_j - \delta_i)\right), \tag{5}$$

$$V_{tj} = \sqrt{\underbrace{\left(x'_{dj}I_{qj}\right)^2}_{V_{dj}} + \underbrace{\left(E'_{qj} - x'_{dj}I_{dj}\right)^2}_{V_{qj}}}, \tag{6}$$

$$P_{ej} = E'_{qj}I_{dj} = \frac{E'_{qj}V_{dj}}{x'_{dj}}, \tag{7}$$

$$Q_{ej} = E'_{qj}I_{dj} = \frac{E'_{qj}V_{qj} - V_{tj}^2}{x'_{dj}}, \tag{8}$$

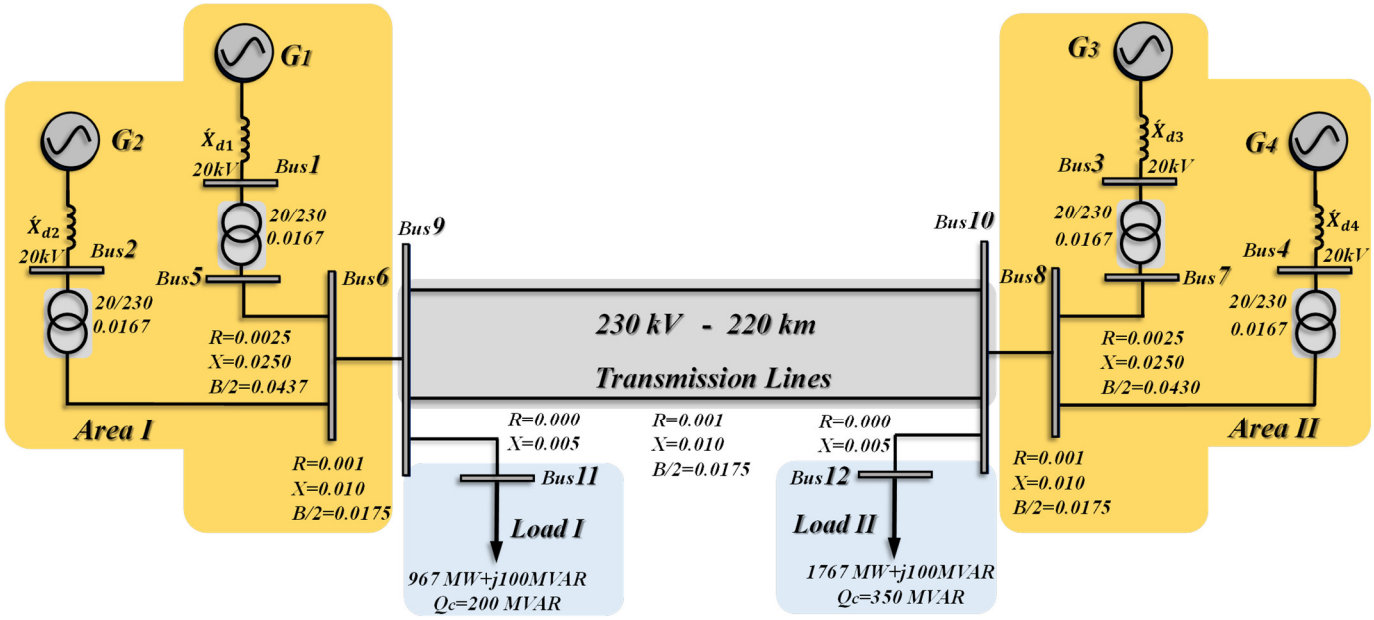

Figure 1. Single-line diagram of a two-area, four-machine power system: a representative example of a multi-machine power system.

Note that the comprehensive list of symbols used in the dynamic model of the multi machine power system is described in Appendix A.

In order to advance a more convenient mathematical calculation, Equations (6) and (7) are incorporated into Equations (2) and (3). Additionally, the variables δ_j, ω_j and E'_{qj} are replaced with x_{1j}, x_{2j} and x_{3j}, respectively. As a result, the dynamics of the *jth* synchronous generator can be expressed as follows:

$$\begin{cases} \dot{x}_{1j} = \xi_{1j} x_{2j} + \eta_{1j} \\ \dot{x}_{2j} = \xi_{2j} x_{3j} + \eta_{2j} \\ \dot{x}_{3j} = \xi_{3j} E_{fdj} + \eta_{3j} \end{cases}, \tag{9}$$

where

$$x_j = \begin{bmatrix} x_{1j} \\ x_{2j} \\ x_{3j} \end{bmatrix}, \ \xi_j = \begin{bmatrix} \xi_{1j} \\ \xi_{2j} \\ \xi_{3j} \end{bmatrix} = \begin{bmatrix} \omega_0 \\ \frac{-\omega_0 I_{qj}}{2H_j} \\ \frac{1}{T'_{d0j}} \end{bmatrix}, \ \eta_j = \begin{bmatrix} \eta_{1j} \\ \eta_{2j} \\ \eta_{3j} \end{bmatrix} = \begin{bmatrix} -\omega_0 \\ \frac{\omega_0}{2H_j} P_{mj} - \frac{D_j}{2H_j} x_{2j} \\ -\frac{1}{T'_{d0j}} \left(x_{3j} + I_{dj} \left(x_{dj} - x'_{dj} \right) \right) \end{bmatrix}, \tag{10}$$

3. Model-Free Excitation System Stabilizer Using the Fractional Calculus Optimization Algorithm

Nowadays, accurately modeling the nonlinearities and dynamic behaviors of modern power systems has become increasingly intricate especially with the growth in these systems' size and diversity. Therefore, model-based control strategies encounter substantial challenges due to the inherent complexities and uncertainties of large-scale power systems. Uncertainties such as the integration of renewable energy and variable load patterns have a high impact on the model's accuracy. Hence, the real-time implementation of model-based control strategies requires continuous model updates, resulting in significant computational resources and scalability concerns. In this section, a practical model-free excitation system stabilizer (MFESS) is developed, utilizing a combination of intelligent proportional integral-derivative (iPID) control, ultra-local control theory and a fractional-order calculus framework. The primary objectives of this control scheme involve enhancing transient and small-signal stability as well as suppressing low-frequency electromechanical oscillations in multi-machine power systems. Note that the proposed model-independent

control framework enhances the control adaptability that renders it a practical choice for complex multi-machine energy systems. Furthermore, a fractional calculus based PSO (FCPSO) optimization algorithm is designed. This optimization algorithm tunes the suggested model-free stabilizer parameters by minimizing the objective function, thereby reducing generator rotor angle deviations.

3.1. Design of an Ultra-Local Controller

An ultra-local model can substitute for the sophisticated mathematical model of the presented multi-machine power system. The dynamics of the energy system can be expressed using the ultra-local model in the model independent control strategy in the following way [45]:

$$F\Big(t,\ x,\ \dot{x},\ \ldots,\ x^{(n)},\ u,\ \dot{u},\ldots,u^{(\ell)}\Big) = 0, \tag{11}$$

where x represents the system's output variable and u denotes the input variable, with $x\ and\ u \in \mathbb{R}$, the function $F(t, x,\ u)$ is sufficiently smooth function of time, and input and output variables. $F(t, x,\ u)$ sufficiently smooth function of time, and input and output variables. The application of the implicit function theorem to Equation (11) facilitates the construction of a local model under the presumption of $\ell,\ n \geq 0, n \geq k,\ k \in \mathbb{Z}^{+}$, and $\frac{\partial F}{\partial x^{(k)}} \not\equiv 0$, as follows:

$$x^{(k)} = \Omega\Big(t,\ x,\ \dot{x},\ \ldots,\ x^{(k-1)}, x^{(k+1)},\ldots, x^{(n)},\ u,\ \dot{u},\ldots,u^{(\ell)}\ \Big), \tag{12}$$

This equation is formulated to segregate and accentuate the elements of uncertainty, the unknown (or insufficiently unknown), and different disturbances in the system. This is achieved by introducing a distinct and continually updated term denoted as g and a non-physical constant represented by $\eta \in \mathbb{R}$ as follows:

$$u^{(k)} = g + \eta u, \tag{13}$$

The model works accurately for a limited amount of time, especially for a sample period that is optimally selected to be as short as feasible to ensure efficient control. The value of g can be derived from the input u and output $x^{(k)}$, expressed as $g^{*} = x^{(k)} - \eta u$, where g^{*} represents the estimated value of the function g. It should be noted that utilizing the control input u in its current presentation is discouraged to prevent the formation of an algebraic loop [46]. Consequently, to rectify this the input u is incorporated into Equation (13) after being subjected to a one-sample time delay, defined as t_s:

$$g^{*}(t) = x^{(k)}(t) - \eta u(t - t_s), \tag{14}$$

To eradicate unknown power system dynamics and achieve an asymptotic reduction in tracking error $\varepsilon^{(k)}(t) = x^{(k)}(t) - x_{ref}^{(k)}(t)$, the construction of the control input can be expanded as follows [47]:

$$u(t) = \frac{1}{\eta}\Big(x_{ref}^{(k)}(t) - g^{*}(t) - E(\varepsilon, t)\Big), \tag{15}$$

where $x_{ref}^{(k)}$ represents the reference tracking signal and $E(\varepsilon, t)$ denotes the feedback controller. If $g^{*}(t)$ closely approximates $g(t)$ $(g^{*}(t) - g(t) \simeq 0)$, indicating the elimination of unknown, and uncertain effects, system stability relies solely on the feedback controller $E(\varepsilon, t)$. Utilizing linear control theory, controller parameters can be selected to track the reference signal $x_{ref}^{(k)}(t)$. By combining Equations (13) and (15), the error dynamics $\varepsilon^{(k)}(t) + E(\varepsilon, t) = 0$ is extracted that ensure asymptotic stability under the given conditions

($\lim_{t\to\infty}\varepsilon(t)=0$) [48]. When employing a PID regulator as the feedback controller, it is referred to as an i-PID regulator [49] with the control input $u(t)$ for i-PID being determined as:

$$u(t)=\frac{x_{ref}^{(\mathscr{k})}(t)-g^{*}(t)-\left(K_D\dot{\varepsilon}(t)+K_I\int\varepsilon(t)dt\right)+K_P\varepsilon(t)}{\eta}, \tag{16}$$

To enhance control performance minimizing the impact of noise and accurately determining $g^{*}(t)$ (as Equation (15)) is crucial. Assuming a sufficiently small sampling time $\mathscr{k}$, the following equation is devised to minimize noise effects and determine Fest, as outlined in [50]:

$$g^{*}=\int_{t-t_s}^{t}\frac{6(t_s-\tau)}{{t_s}^3}(x(\tau)+\eta\tau u(\tau))d\tau, \tag{17}$$

An alternative equation for determining Fest is obtained by rearranging Equation (14) as $g^{*}(t)=x^{(\mathscr{k})}(t)-\eta u(t-t_s)$. Calculating the $\mathscr{k}$-th derivative of the system output, $x^{(\mathscr{k})}(t)$, facilitates the computation of $g^{*}(t)$. The system and the practitioner determine which derivative order to use. Computational efficiency and control performance are trade-offs, while a higher derivative order can improve control performance, it may also provide computational difficulties. In order to handle this trade-off, the following term is proposed in place of specifying the ideal derivative operator $X(s)=s$ which is improper and would not yield trustworthy results in physical systems:

$$X(s)=\frac{\mathscr{f}s}{s+\mathscr{f}}, \tag{18}$$

where $\mathscr{f}>0$ denotes a positive factor. As $\mathscr{f}$ approaches infinity ($\mathscr{f}\to\infty$), $X(s)$ merges with the ideal derivative function. This technique enables the estimation of the $\mathscr{k}^{th}$ derivative of the system output $x^{(\mathscr{k})}(t)$, as follows:

$$x^{*(\mathscr{k})}(s)=X^{(\mathscr{k})}(s)x(s), \tag{19}$$

In the transient solution of a specific signal in the control system, a fundamental element is represented by $e^{\gamma t}$. By choosing $x(t)=e^{\gamma t}$, the estimated first derivative of the control system output is given by:

$$\dot{x}^{*}(t)=\frac{\mathscr{f}}{\gamma+\mathscr{f}}\left(\mathscr{f}e^{-\mathscr{f}t}-\gamma e^{-\gamma t}\right), \tag{20}$$

Utilizing Equation (15) and selecting the first derivative of the control output ($\dot{x}(t)=\gamma e^{\gamma t}$), the tracing error function can be computed using the following numerical derivative expression [50]:

$$\varepsilon(t)=\frac{1}{\dot{x}(t)}\left|\dot{x}^{*}(t)-\dot{x}(t)\right|, \tag{21}$$

However, the presented error value indicated in Equation (21) inversely varies with the factor $\mathscr{f}$. Note that, it becomes zero when $\mathscr{f}$ tends to infinity ($\mathscr{f}\to\infty$). The study also demonstrates effectiveness for higher derivative orders, as $\left\{\lim_{\mathscr{f}\to\infty}\varepsilon(t,\mathscr{f})=0,\forall t,\ |\gamma|\in(0,\infty)\right\}$. In addition to this procedure, Newton's difference quotient is a fundamental approach for taking derivatives. When the noise level is low or effectively eliminated with a low pass filter, a numerical derivative equation can be applied as follows [50]:

$$\dot{x}(t)=\frac{1}{t_s}(x(t)-x(t-t_s)), \tag{22}$$

The suggested control strategy is built on Newton's difference quotient technique for derivative calculation with factors. In the first step, a low-pass filter has already been

applied to the system output, reducing the signal's noise, and making it acceptable for this procedure. Further, to ensure precise computations, a sufficiently small sample duration, $\mathcal{k}$, has been selected. In addition, the system model's order makes it sufficient to choose $n = 1$, that is, the first derivative of the system output $\dot{x}(t)$.

3.2. Fractional Calculus-Based Particle Swarm Optimization (FCPSO) Algorithm

Based on Equation (11) the control inputs of $u(t)$ is affected by control coefficients K_D, K_I, and K_P. Therefore, optimizing the control coefficients of the proposed model-free controller is crucial. Note that tuning the parameters of the presented control framework can guarantee optimal performance and stability in the multi-machine power system. Properly tuned parameters can also enhance responsiveness, minimize overshoot, and reduce settling time, thereby improving the system's ability to accurately track desired setpoints and reject disturbances. In order to optimize the performance of the designed controller, a fractional calculus-based particle swarm optimization (PSO) algorithm is employed.

PSO is a stochastic optimization method based on social simulation models inspired by rules regulating coordinated behaviors in real populations such as fish groups, animal herds, and flocks of birds. Its increasing popularity is due to several special features, such as simple implementation, independence from gradient information, dependency only on values of the objective function, adaptability to high-dimensional multi-optima and nonlinear problems, and robustness to initial particle states. The efficiency of the PSO algorithm is demonstrated through a diverse analysis in different fields in comparison with the other optimization frameworks. Illustrated in Algorithm 1 is a typical PSO algorithm, portraying its fundamental operations with a random initialization of the swarm within the search space [45,51].

The provided pseudocode in Algorithm 1 is denoted by t with $t + 1$ that represent the successive iteration. Position ($\varkappa$) of each particle evolves by counting a velocity term (v). This velocity is determined by adding an increment to the previous velocity value, which is computed based on two components representing cognitive and social knowledge. Each particle's cognitive knowledge is determined by comparing its current position, $\varkappa$, with the best position it has discovered, ℓ. Meanwhile, the social knowledge of each particle considers the disparity between its current position, $\varkappa$, and the best global position the swarm has attained, ϖ_b [52].

Algorithm 1

set the population size and dimension
set the searching space
initialize swarm
repeat
for all particles do
calculate fitness function values
end
for all particles do
$v_{t+1} = v_t + \mu_1(\ell - \varkappa) + \mu_2(\varpi_b - \varkappa)$
$\varkappa_{t+1} = \varkappa_t + v_{t+1}$
end
$t = t + 1$
until stopping rule

By randomly generated terms μ_1 and μ_2 the cognitive and social factors are weighted. PSO stands for a powerful optimization algorithm known for its efficiency, robustness and simplicity. Thus, without careful consideration, velocities within the algorithm can escalate, especially when particles are distant from local to global bests. Among the different

strategies that have been explored in the literature to mitigate this problem, Eberhart et al. introduced a clamping function to restrict velocity, defined by the expression [53]:

$$v_{ij,\,t+1} = \begin{cases} v_{max,j}, & where \quad \acute{v}_{ij,\,t+1} \geq v_{max,j} \\ \acute{v}_{ij,\,t+1}, & where \quad \acute{v}_{ij,\,t+1} < v_{max,j} \end{cases}, \tag{23}$$

where $\acute{v}_{ij,\,t+1}$ is equal to $\Im v_{ij,\,t} + \mu_1(\ell - \varkappa) + \mu_2(\circ_b - \varkappa)$ for the parameter j of the particle i at iteration $t + 1$. In addition, $\Im$ is the inertia weighting coefficient that shows the convergence rate over each evolution, as follows:

$$v_{\,t+1} = \Im v_t + \mu_1(\ell - \varkappa) + \mu_2(\circ_b - \varkappa), \tag{24}$$

Fractional calculus has its roots in the theory of differential calculus and has gained significant attention in the past two decades driven by advances in nonlinear and complex systems. While some work has been done in the field of dynamic systems theory, models and algorithms are still in the early stages of development. The foundational aspects of FC theory are extensively discussed in the literature. FC extends the concept of derivative and integral to non-integer order $\wp$ defined using the Grünwald-Letnikov definition as follows:

$$D^{\wp}[Z(t)] = \frac{1}{T_{FC}} \sum_{\rho=0}^{q} \frac{(-1)^{\rho} Z(\mathrm{t} - \rho T_{FC}) \Gamma(\wp + 1)}{\Gamma(\wp - \rho + 1)\Gamma(\rho + 1)}, \tag{25}$$

where q denotes the truncation order. Also, T_{FC} stands for the sampling period in Equation (25). This definition highlights the key difference between integer and fractional derivatives: while integer derivatives are 'local' operators' fractional derivatives inherently possess a 'memory' of past events. This is due to their requirement for an infinite series of terms.

The following $\mathcal{Z}$-transform formulation provides a direct generalization of the classical integer-order scheme for fractional derivatives, which is well-suited for describing phenomena such as irreversibility and chaos due to its memory property [54]:

$$\mathcal{Z}\{D^{\wp}[Z(t)]\} = \left(\frac{1 - \mathfrak{D}^{-1}}{T_{FC}}\right)^{\wp} Z(\mathfrak{D}), \tag{26}$$

where $\mathfrak{D}$ is the variable of the $\mathcal{Z}$-transform function. The fractional-order model property makes FC tools suitable for modeling the propagation of perturbations and long-term dynamic phenomena in evolving populations.

In this step, the fractional calculus-based particle swarm optimization (FCPSO) algorithm is employed to adjust the parameters of the model-free control framework presented in Part A. By combining the velocity update rule Equation (24) and the Grünwald-Letnikov equation the position term $(\ell - \varkappa)$ can be extracted as follows:

$$\ell - \varkappa_{t+1} = \ell - \wp\varkappa_t - \frac{\wp(1-\wp)}{2}\varkappa_{t-1} - \frac{\wp(1-\wp)(2-\wp)}{6}\varkappa_{t-2} - \frac{\wp(1-\wp)(2-\wp)(3-\wp)}{24}\varkappa_{t-3}, \tag{27}$$

Note that Equation (27) is expanded based on the first four terms of the fractional derivative series ($q = 4$). As depicted in Figure 2, the local feedback of the particle position $\varkappa_t$ is modified by fractional feedback in the FCPSO structure. By using the characteristics of the Gamma function ($\Gamma(\wp + 1) = \wp\Gamma(\wp) = \wp(\wp - 1)\Gamma(\wp - 1)\Gamma(\wp + 1) = \wp(\wp - 1)(\wp - 2)\Gamma(\wp - 2)$) and $\Gamma(1) = 1$, $\Gamma(2) = 1$, $\Gamma(3) = 2$, $\Gamma(4) = 6$, $\Gamma(5) = 24$, the final velocity update low for the FCPSO can be described as:

$$\begin{aligned} v_{t+1} = \Im v_t + \mu_2(\circ_b - \varkappa_t) + \mu_1(\ell - \wp\varkappa_t - \tfrac{\wp(1-\wp)}{2}\varkappa_{t-1} - \\ \tfrac{\wp(1-\wp)(2-\wp)}{6}\varkappa_{t-2} - \tfrac{\wp(1-\wp)(2-\wp)(3-\wp)}{24}\varkappa_{t-3}), \end{aligned} \tag{28}$$

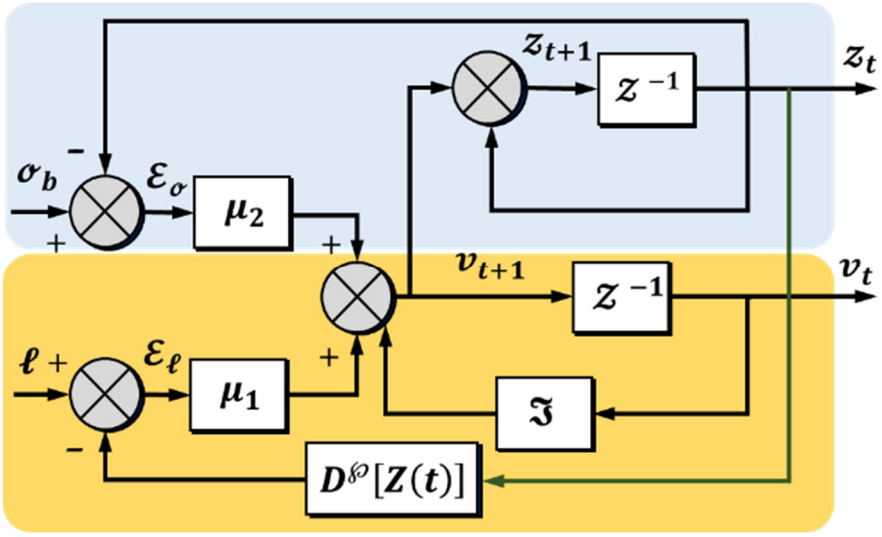

Figure 2. Block diagram of the presented FCPSO algorithm (ε_σ: global error, and ε_ℓ: local error).

Note that the presented FCPSO algorithm has been employed to optimally tune the design parameters of the suggested MFES (K_D, K_I and K_P). To define an effective objective function, the integral of time absolute error (ITAE) is considered a constrained optimization framework as follows:

$$Minimize\ ITAE = \int_0^{t_{sim}} t.|\Delta\omega|.dt, \tag{29}$$

Subjected to:

$$K_D^{min} \le K_D \le K_D^{max}, \tag{30}$$

$$K_I^{min} \le K_I \le K_I^{max}, \tag{31}$$

$$K_P^{min} \le K_P \le K_P^{max}, \tag{32}$$

The proposed control framework is depicted in Figure 3. As mentioned in Section 2, the main goal of the presented control framework is to enhance transient stability and suppress low-frequency electromechanical oscillations within the multimachine energy system. Therefore, for the dynamics of the *jth* generation unit, presented in Equations (1)–(10), the input control reference in Figure 3 is the reference value of the rotor speed of the *jth* generator.

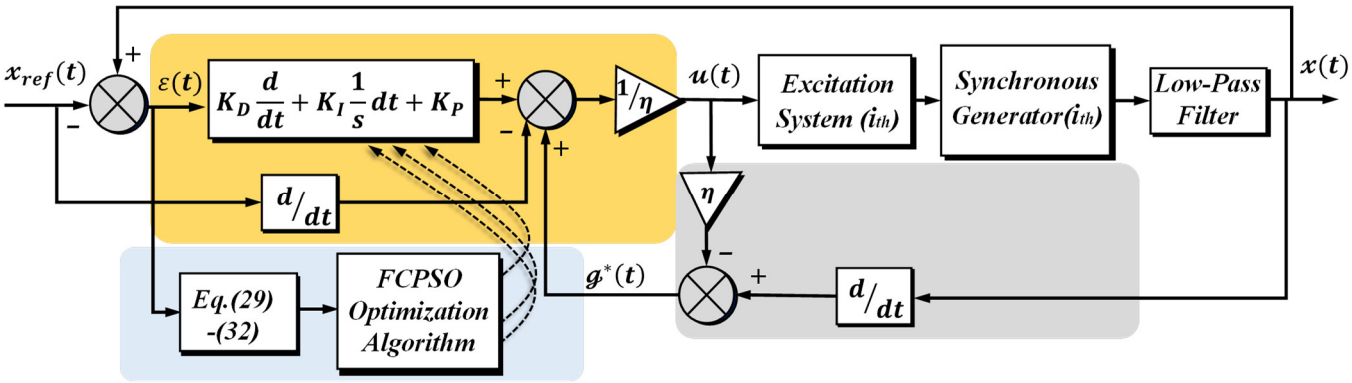

Figure 3. Block diagram of MFESS with supplementary FCPSO parameter adaptation algorithm.

4. Simulation Results

This part conducts a comprehensive numerical analysis to demonstrate the effectiveness of the proposed optimal fractional-based model-free approach. Numerical analysis

is conducted on the presented two-area four-machine power system. As depicted in Figure 1, this system comprises two areas each housing two generators rated at 900 MW and 20 kV [43]. These two areas are interconnected by two identical 230 kV transmission lines with a total length of 440 km. Each generator is linked to a 230 kV transmission line via transformers. These generation units transfer 400 MV from Area 1 to Area 2 [54]. The parameters of the synchronous machines utilized in the simulation are: $x'_{dj} = 0.3$ pu, $x_{dj} = 1.8$ pu, $x_{qj} = 1.7$ pu, $\acute{x}_{qj} = 0.55$ pu, $R_{sj} = 0.0025$ pu, $x_1 = 0.2$ pu, $T'_{d0j} = 0.4$ s [43]. To validate the efficacy of the proposed model-free excitation system stabilizer (MFESS) integrated with the fractional calculus-based particle swarm optimization (FCPSO) algorithm, termed FCPSO-MFESS, simulation results of this framework are compared with those obtained from conventional excitation systems comprising a conventional power system stabilizer and automatic voltage regulator (CPSS-AVR). Additionally, comparisons are made with the proposed MFESS framework devoid of parameter tuning schemes (MFESS) and a particle swarm optimization-based MFESS (PSO-MFESS).

The standard block diagram of the conventional excitation system (CPSS-AVR), which includes the washout filter, limiters, and two lead-lag compensation networks, is illustrated in Figure 4. The parameters of the conventional excitation system (with AVR) for each generator are: $K_{Ai} = 300$, $T_{Ai} = 0.001\ s$, $T_{Bi} = 2\ s$, $T_{Ci} = 10\ s$. Moreover, the parameters of the CPSS for each machine are summarized in Table 1 [55].

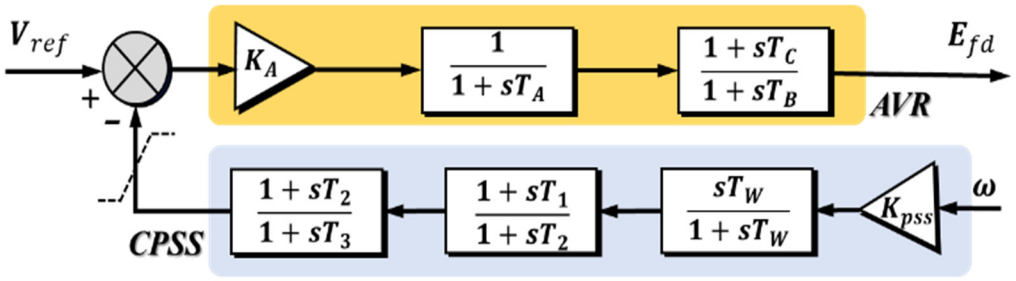

Figure 4. The standard block diagram of the conventional excitation system (CPSS-AVR).

Table 1. Parameters of conventional excitation systems.

G_i	$K_{CPSS,\,i}$	$T_{1CPSS,\,i}$	$T_{2CPSS,\,i}$	$T_{3CPSS,\,i}$	$T_{4CPSS,\,i}$
G_1	10.81	0.913	0.038	0.723	0.213
G_2	20.22	0.310	0.066	0.878	0.019
G_3	7.025	0.516	0.112	1.400	0.015
G_4	9.442	1.422	0.045	0.456	0.050

Figure 5 illustrates the responses of the multi-machine power system to a three-phase short-circuit fault (large disturbance) occurring at t = 0 s along one of the two 220 km lines between Buses 9 and 10. The fault persists in the system for 0.15 s before being rectified. The control parameters of the MFESS are:

$K_D = 0.3051$, $K_I = 0.8010$, $K_P = 1.2048$. Furthermore, the optimal settings for the PSO-MFESS and FCPSO-MFESS stabilizers are $K_D = 0.2062$, $K_I = 0.5097$, $K_P = 0.9028$ and $K_D = 0.2643$, $K_I = 0.4706$, $K_P = 0.8502$, respectively. Comparative analysis with other configurations (CPSS-AVR, MFESS, and PSO-MFESS) reveals that the system integrated with the FCPSO-MFESS exhibits superior performance in terms of transient and small-signal stability, effectively damping low-frequency electromechanical oscillations.

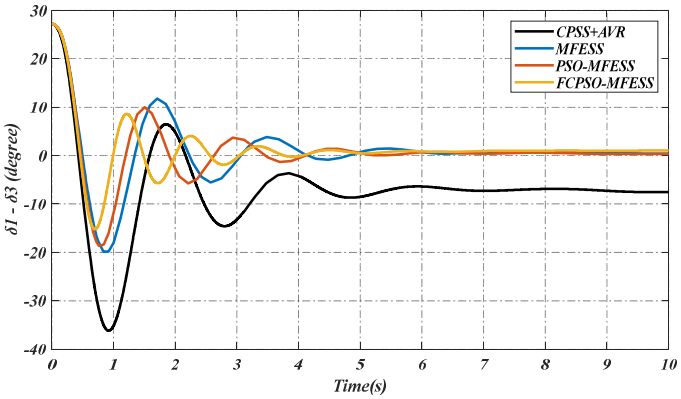

(**a**) Relative rotor angle response δ_{13} (degree)

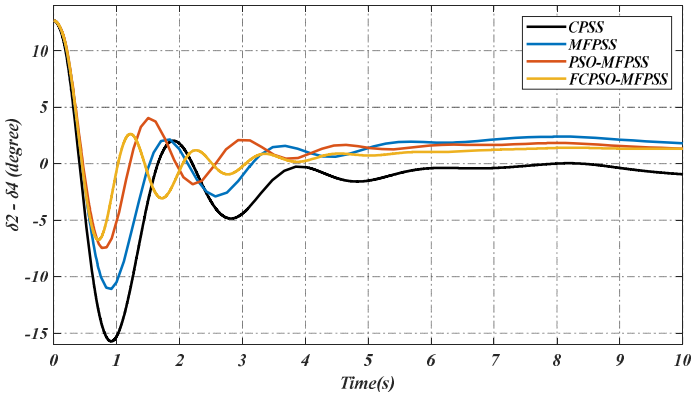

(**b**) Relative rotor angle response δ_{24} (degree)

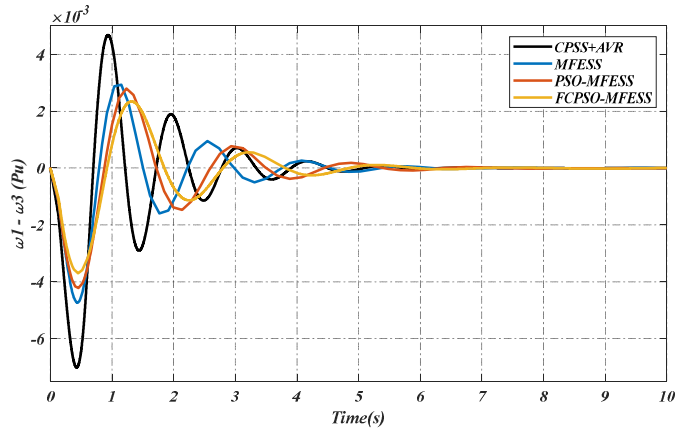

(**c**) Relative rotor speed response ω_{13} (p.u.)

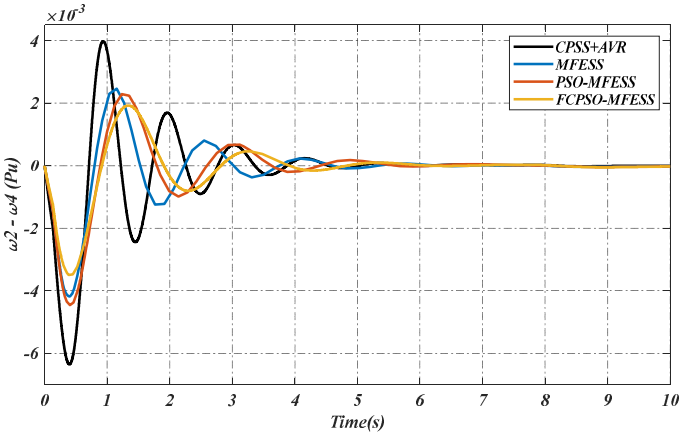

(**d**) Relative rotor angle response ω_{24} (p.u.)

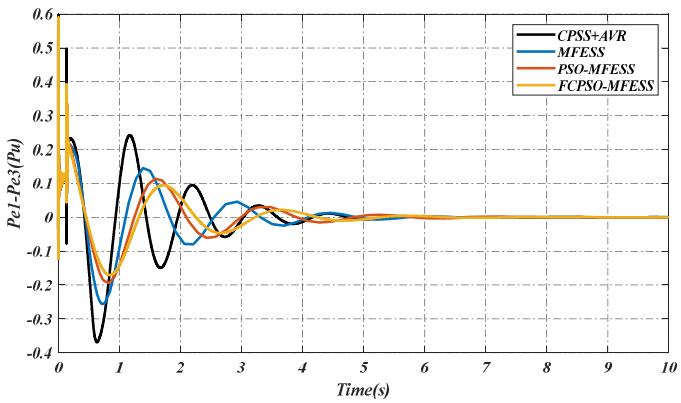

(**e**) Relative active power P_{13} (p.u.)

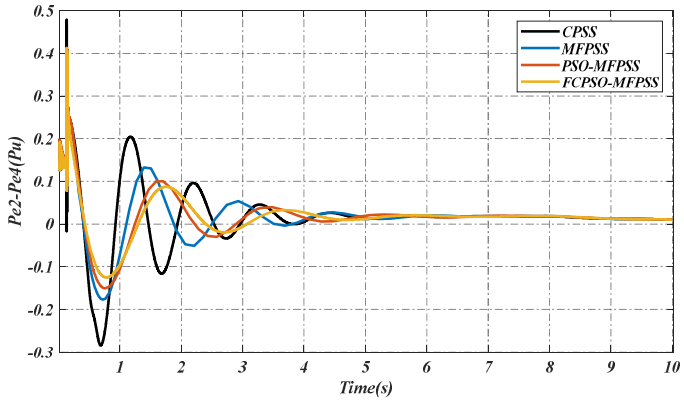

(**f**) Relative active power P_{24} (p.u.)

Figure 5. Multi machine power system responses to a three-phase short-circuit fault (large disturbance).

Figure 5a depicts the relative rotor angle response between the first and third generators, demonstrating the effective operation of the proposed FCPSO-MFESS control framework in managing overshoot, undershoot, and settling time compared to other cases. For example, this comparison shows that the suggested control approach in this paper can reduce the undershoot of the first wave relative rotor angle and its settling time to −15.18 degrees and 6 s, respectively, from −36.161 degrees and 10 s in the CPSS-AVR case, representing a 58.05% reduction in undershoot and a 40% reduction in settling time. Figure 5b illustrates disparities in rotor angle responses between the second and fourth synchronous generators. These results also demonstrate the effective control behavior of the presented FCPSO-MFESS.

Moreover, Figure 5c,d present the relative rotor angle responses of first-to-third-generation units, and second-to -fourth generation units respectively. A comparative examination indicates that both PSO-MFESS and FCPSO-MFESS significantly enhance system transient stability compared to MFESS and traditional excitation systems. For example, in Figure 5d, the first wave overshoot and undershoot of the speed response reduce to 0.003493 p.u. and 0.0019236 p.u., respectively, from 0.006341 p.u. to 0.003979 p.u. in the CPSS-AVR case, representing a 44.95% reduction in overshoot and a 51.69% reduction in first wave undershoot. Furthermore, FCPSO-MFESS demonstrates superior performance over PSO-MFESS, underscoring the efficacy of the parameter adaptation technique based on fractional calculus. Specifically, PSO-MFESS facilitates faster attainment of a new equilibrium state for generator rotor angle and rotor speed while efficiently dampening oscillations. The control operation of the proposed FCPSO-MFESS framework effectively dampens oscillations in the relative active power of generation units within the same and opposite areas of the multimachine power system. These results, depicted in Figure 5e,f, demonstrate the effective performance of the suggested intelligent model-free approach in this paper.

5. Conclusions

This paper introduces a novel and practical model-free fractional calculus-based excitation system stabilizer. It is strategically devised to tackle the inherent challenges of modern energy systems. By harnessing principles of ultra-local control and fractional-order calculus the proposed stabilizer aims to enhance transient performance and mitigate low-frequency electromechanical oscillations in multimachine power systems. The integration of fractional calculus-based particle swarm optimization algorithms amplifies stabilizer efficacy. This algorithm fine-tunes the controller parameters to adapt to diverse operational conditions. Diverse numerical analyses have been conducted on a two-area multi-machine power system to demonstrate the effectiveness of the proposed control framework over conventional controllers in terms of transient and small-signal stability. The results show that the suggested control strategy in this work is capable of maintaining transient stability and suppressing low-frequency oscillations in multi-machine power systems. This research represents a significant advancement in the realm of model-independent control strategies tailored to the intricacies and uncertainties of modern energy systems. It thereby contributes to the optimization of power system efficiency and enhances stability. Due to the learning-based nature of the machine learning-based optimization algorithms, future research will include exploring how deep reinforcement learning algorithms can be used as a parameter in the proposed model independent control framework.

Author Contributions: Conceptualization, A.F. and B.A.; Methodology, A.F. and B.A.; Validation, A.F. and B.A.; Investigation, A.F.; Writing—original draft, A.F.; Writing—review & editing, B.A.; Supervision, B.A. All authors have read and agreed to the published version of the manuscript.

Funding: This research received no external funding.

Data Availability Statement: Data are contained within the article.

Conflicts of Interest: The authors declare no conflict of interest.

Appendix A. List of Symbols of the Dynamic Model of a Multi-Machine Power System

In this appendix, the comprehensive list of symbols utilized in the dynamic model of the multi-machine power system is illustrated as follows:

T'_{d0j}	*D*-axis open circuit field time constant
ω_j	Rotor speed of the *jth* synchronous generator
ω_0	Synchronous speed of the synchronous generators
ω_{ref}	Rotor speed reference value of the *jth* synchronous generator
δ_j	Rotor angle of the *jth* synchronous generator
D_j	Mechanical damping coefficient of the *jth* synchronous generator
H_j	Inertia constant of the *jth* synchronous generator
P_{mj}	Mechanical power input to the *jth* synchronous generator shaft
P_{ej}	Active electrical power output of the *jth* synchronous generator
E'_{qj}	Transient q-axis electromechanical force (EMF) of the *jth* synchronous generator
E_{fdj}	Equivalent electro-motive force (EMF) in excitation winding of the *jth* synchronous generator
x_{dj}	Direct-axis reactance of the *jth* synchronous generator
x'_{dj}	Direct-axis transient reactance of the *jth* synchronous generator
I_{dj}	Direct-axis stator current of the *jth* synchronous generator
I_{qj}	Quadrature-axis stator current of the *jth* synchronous generator
V_{tj}	Terminal voltage of the *jth* synchronous generator
V_{dj}, V_{qj}	q and d-axis of the *jth* synchronous generator stator voltages

References

1. Zhang, N.; Jia, H.; Hou, Q.; Zhang, Z.; Xia, T.; Cai, X.; Wang, J. Data-Driven Security and Stability Rule in High Renewable Penetrated Power System Operation. *Proc. IEEE* **2023**, *111*, 788–805. [CrossRef]
2. Du, W.; Fu, Q.; Wang, H.F. Power System Small-Signal Angular Stability Affected by Virtual Synchronous Generators. *IEEE Trans. Power Syst.* **2019**, *34*, 3209–3219. [CrossRef]
3. Prakash, A.; Moursi, M.S.E.; Parida, S.K.; Kumar, K.; El-Saadany, E.F. Damping of Inter-Area Oscillations with Frequency Regulation in Power Systems Considering High Penetration of Renewable Energy Sources. *IEEE Trans. Ind. Appl.* **2024**, *60*, 1665–1679. [CrossRef]
4. Liccardo, A.; Tessitore, S.; Bonavolontà, F.; Cristiano, S.; Noia, L.P.D.; Giannuzzi, G.M.; Pisani, C. Detection and Analysis of Inter-Area Oscillations Through a Dynamic-Order DMD Approach. *IEEE Trans. Instrum. Meas.* **2022**, *71*, 1–14. [CrossRef]
5. Fathollahi, A.; Andresen, B. Deep Deterministic Policy Gradient for Adaptive Power System Stabilization and Voltage Regulation. *E-Prime Adv. Electr. Eng. Electron. Energy* **2024**, *9*, 100675. [CrossRef]
6. Alaraifi, S.; Djouadi, S.; Moursi, M.S.E. Domain of Stability Characterization for Power Systems: A Novel Individual Invariance Method. *IEEE Trans. Power Syst.* **2024**, *39*, 14–27. [CrossRef]
7. Oshnoei, S.; Fathollahi, A.; Oshnoei, A.; Khooban, M.H. Microgrid Frequency Regulation Based on a Fractional Order Cascade Controller. *Fractal Fract.* **2023**, *7*, 343. [CrossRef]
8. Mira-Gebauer, N.; Rahmann, C.; Álvarez-Malebrán, R.; Vittal, V. Review of Wide-Area Controllers for Supporting Power System Stability. *IEEE Access* **2023**, *11*, 8073–8095. [CrossRef]
9. Wang, G.; Tang, Y.; Li, Y.; Ai, D.; Chen, G.; Wei, W. Control Method for Additional Damper in Hydro-turbine Speed Governor of Hydro-dominant Power Systems. *CSEE J. Power Energy Syst.* **2023**, *9*, 589–598. [CrossRef]
10. Zamani, M.; Shahgholian, G.; Fathollahi, A.; Mosavi, A.; Felde, I. Improving Interarea Mode Oscillation Damping in Multi-Machine Energy Systems through a Coordinated PSS and FACTS Controller Framework. *Sustainability* **2023**, *15*, 16070. [CrossRef]
11. Du, W.; Dong, W.; Wang, Y.; Wang, H. A Method to Design Power System Stabilizers in a Multi-Machine Power System Based on Single-Machine Infinite-Bus System Model. *IEEE Trans. Power Syst.* **2021**, *36*, 3475–3486. [CrossRef]
12. Shahgholian, G.; Fattollahi, A. Improving power system stability using transfer function: A comparative analysis. *Eng. Technol. Appl. Sci. Res.* **2017**, *7*, 1946–1952. [CrossRef]
13. Bhadu, M.; Senroy, N.; Narayan Kar, I.; Sudha, G.N. Robust linear quadratic Gaussian-based discrete mode wide area power system damping controller. *IET Gener. Transm. Distrib.* **2016**, *10*, 1470–1478. [CrossRef]
14. Fregene, K.; Kennedy, D. Stabilizing control of a high-order generator model by adaptive feedback linearization. *IEEE Trans. Energy Convers.* **2003**, *18*, 149–156. [CrossRef]
15. Mansour, M.Z.; Ravanji, M.H.; Karimi, A.; Bahrani, B. Small-Signal Synchronization Stability Enhancement of Grid-Following Inverters via a Feedback Linearization Controller. *IEEE Trans. Power Deliv.* **2022**, *37*, 4335–4344. [CrossRef]
16. Bento, M.E.C.; Ramos, R.A. A Method Based on Linear Matrix Inequalities to Design a Wide-Area Damping Controller Resilient to Permanent Communication Failures. *IEEE Syst. J.* **2021**, *15*, 3832–3840. [CrossRef]
17. Zucco, J.P.T.; Ramirez, H.; Wu, Y.; Gorrec, Y.L. Linear Matrix Inequality Design of Exponentially Stabilizing Observer-Based State Feedback Port-Hamiltonian Controllers. *IEEE Trans. Autom. Control* **2023**, *68*, 6184–6191. [CrossRef]

18. Sun, Z.; Cao, Y.; Wen, Z.; Song, Y.; Sun, Z. A Grey Wolf Optimizer algorithm based fuzzy logic power system stabilizer for single machine infinite bus system. *Energy Rep.* **2023**, *9*, 847–853. [CrossRef]
19. Ansari, J.; Abbasi, A.R.; Heydari, M.H.; Avazzadeh, Z. Simultaneous design of fuzzy PSS and fuzzy STATCOM controllers for power system stability enhancement. *Alex. Eng. J.* **2022**, *61*, 2841–2850. [CrossRef]
20. Kumar, A. Power System Stabilizers Design for Multimachine Power Systems Using Local Measurements. *IEEE Trans. Power Syst.* **2016**, *31*, 2163–2171. [CrossRef]
21. Fattollahi, A.; Dehghani, M.; Yousefi, M.R. Analysis and simulation dynamic behavior of power system equipped with PSS and excitation system stabilizer. *Signal Process. Renew. Energy* **2022**, *6*, 99–111.
22. Roy, T.K.; Mahmud, M.A.; Shen, W.; Oo, A.M.T. A non-linear adaptive excitation control scheme for feedback linearized synchronous generations in multimachine power systems. *IET Gener. Transm. Distrib.* **2021**, *15*, 1501–1520. [CrossRef]
23. Shi, L.; Lee, K.Y.; Wu, F. Robust ESS-Based Stabilizer Design for Damping Inter-Area Oscillations in Multimachine Power Systems. *IEEE Trans. Power Syst.* **2016**, *31*, 1395–1406. [CrossRef]
24. Han, W.; Stanković, A.M. Model-Predictive Control Design for Power System Oscillation Damping via Excitation—A Data-Driven Approach. *IEEE Trans. Power Syst.* **2023**, *38*, 1176–1188. [CrossRef]
25. Halder, A.; Pal, N.; Mondal, D. Higher order sliding mode STATCOM control for power system stability improvement. *Math. Comput. Simul.* **2020**, *177*, 244–262. [CrossRef]
26. Farahani, M.; Ganjefar, S. Intelligent power system stabilizer design using adaptive fuzzy sliding mode controller. *Neurocomputing* **2017**, *226*, 135–144. [CrossRef]
27. Musarrat, M.N.; Fekih, A. A fractional order sliding mode control-based topology to improve the transient stability of wind energy systems. *Int. J. Electr. Power Energy Syst.* **2021**, *133*, 107306. [CrossRef]
28. Liao, K.; He, Z.; Xu, Y.; Chen, G.; Dong, Z.Y.; Wong, K.P. A Sliding Mode Based Damping Control of DFIG for Interarea Power Oscillations. *IEEE Trans. Sustain. Energy* **2017**, *8*, 258–267. [CrossRef]
29. Lee, S.S.; Li, S.Y.; Park, J.K. Nonlinear adaptive back-stepping controller design for power system stabilizer in multi-machine power systems. In Proceedings of the 2008 American Control Conference, Seattle, WA, USA, 11–13 June 2008; pp. 2504–2509. [CrossRef]
30. Zhao, P.; Yao, W.; Wen, J.; Jiang, L.; Wang, S.; Cheng, S. Improved synergetic excitation control for transient stability enhancement and voltage regulation of power systems. *Int. J. Electr. Power Energy Syst.* **2015**, *68*, 44–51. [CrossRef]
31. Fattollahi-Dehkordi, A.; Shahgholian, G.; Fani, B. Decentralized synergistic control of multi-machine power system using power system stabilizer. *Signal Process. Renew. Energy* **2020**, *4*, 1–21.
32. Mir, A.S.; Singh, A.K.; Pal, B.C.; Senroy, N.; Tu, J. Adequacy of Lyapunov Control of Power Systems Considering Modelling Details and Control Indices. *IEEE Trans. Power Syst.* **2023**, *38*, 2275–2289. [CrossRef]
33. Ospina, L.D.P.; Salazar, V.U.; Ospina, D.P. Dynamic Equivalents of Nonlinear Active Distribution Networks Based on Hammerstein-Wiener Models: An Application for Long-Term Power System Phenomena. *IEEE Trans. Power Syst.* **2022**, *37*, 4286–4296. [CrossRef]
34. Zhao, J.; Zhang, Y.; Wang, X. Model-Free Predictive Current Control of PMSM Drives Based on Variable Sequence Space Vector Modulation Using an Ultra-Local Model. *IEEE Trans. Transp. Electrif.* **2024**, *10*, 3518–3528. [CrossRef]
35. Fathollahi, A.; Gheisarnejad, M.; Andresen, B.; Farsizadeh, H.; Khooban, M.-H. Robust artificial intelligence controller for stabilization of full-bridge converters feeding constant power loads. *IEEE Trans. Circuits Syst. II Express Briefs* **2023**, *70*, 3504–3508. [CrossRef]
36. Wang, B.; Fan, H.; Li, Z.; Feng, G.; Han, Y. An Ultra-Local Model-Based Control Method with the Bus Voltage Supervisor for Hybrid Energy Storage System in Electric Vehicles. *IEEE J. Emerg. Sel. Top. Power Electron.* **2024**, *12*, 461–471. [CrossRef]
37. Hou, Z.; Lei, T. Constrained Model Free Adaptive Predictive Perimeter Control and Route Guidance for Multi-Region Urban Traffic Systems. *IEEE Trans. Intell. Transp. Syst.* **2022**, *23*, 912–924. [CrossRef]
38. Ren, J.C.; Liu, D.; Wan, Y. Model-Free Adaptive Iterative Learning Control Method for the Czochralski Silicon Monocrystalline Batch Process. *IEEE Trans. Semicond. Manuf.* **2021**, *34*, 398–407. [CrossRef]
39. Fliess, M.; Join, C. Intelligent PID controllers. In Proceedings of the 2008 16th Mediterranean Conference on Control and Automation, Ajaccio, France, 25–27 June 2008; pp. 326–331. [CrossRef]
40. Wang, H.P.; Mustafa, G.I.Y.; Tian, Y. Model-free fractional-order sliding mode control for an active vehicle suspension system. *Adv. Eng. Softw.* **2018**, *115*, 452–461. [CrossRef]
41. Younes, Y.A.; Drak, A.; Noura, H.; Rabhi, A.; Hajjaji, A.E. Model-free control of a quadrotor vehicle. In Proceedings of the 2014 International Conference on Unmanned Aircraft Systems (ICUAS), Orlando, FL, USA, 27–30 May 2014; pp. 1126–1131. [CrossRef]
42. Huang, S.; Xiong, L.; Wang, J.; Li, P.; Wang, Z.; Ma, M. Fixed-Time Fractional-Order Sliding Mode Controller for Multimachine Power Systems. *IEEE Trans. Power Syst.* **2021**, *36*, 2866–2876. [CrossRef]
43. Kundur, P. *Power System Stability and Control*; McGraw-Hill: New York, NY, USA, 2007.
44. Fathollahi, A.; Kargar, A.; Derakhshandeh, S.Y. Enhancement of power system transient stability and voltage regulation performance with decentralized synergetic TCSC controller. *Int. J. Electr. Power Energy Syst.* **2022**, *135*, 107533. [CrossRef]
45. Long, B.; Zhang, J.; Shen, D.; Rodríguez, J.; Guerrero, J.M.; Chong, K.T. Ultralocal Model-Free Predictive Control of T-Type Grid-Connected Converters Based on Extended Sliding-Mode Disturbance Observer. *IEEE Trans. Power Electron.* **2023**, *38*, 15494–15508. [CrossRef]

46. Fliess, M. Model-free control and intelligent PID controllers: Towards a possible trivialization of nonlinear control? *IFAC Proc.* **2009**, *42*, 1531–1550. [CrossRef]
47. Mosayebi, M.; Fthollahi, A.; Gheisarnejad, M.; Farsizadeh, H.; Khooban, M.H. Smart Emergency EV-to-EV Portable Battery Charger. *Inventions* **2022**, *7*, 45. [CrossRef]
48. Fliess, M.; Join, C. Stability margins and model-free control: A first look. In Proceedings of the 2014 European Control Conference (ECC), Strasbourg, France, 24–27 June 2014; pp. 454–459.
49. Coskun, M.Y.; İtik, M. Intelligent PID control of an industrial electro-hydraulic system. *ISA Trans.* **2023**, *139*, 484–498. [CrossRef]
50. Wang, Q.-G.; Liu, T.; Nie, Z.-Y.; Hao, S.; Ren, X.; Zhang, D.; Wang, L. A generalized control scheme for system uncertainty estimation and cancellation. *Trans. Inst. Meas. Control* **2021**, *43*, 2921–2933. [CrossRef]
51. Jeong, Y.W.; Park, J.B.; Jang, S.H.; Lee, K.Y. A New Quantum-Inspired Binary PSO: Application to Unit Commitment Problems for Power Systems. *IEEE Trans. Power Syst.* **2010**, *43*, 1486–1495. [CrossRef]
52. Hong, Y.Y.; Hsiao, C.Y. Under-Frequency Load Shedding in a Standalone Power System with Wind-Turbine Generators Using Fuzzy PSO. *IEEE Trans. Power Deliv.* **2022**, *37*, 1140–1150. [CrossRef]
53. Ferreira, N.M.F.; Machado, J.A.T. *Mathematical Methods in Engineering*; Springer: Dordrecht, The Netherlands, 2014.
54. Fathollahi, A.; Andresen, B. Multi-Machine Power System Transient Stability Enhancement Utilizing a Fractional Order-Based Nonlinear Stabilizer. *Fractal Fract.* **2023**, *7*, 808. [CrossRef]
55. Keumarsi, V.; Simab, M.; Shahgholian, G. An integrated approach for optimal placement and tuning of power system stabilizer in multi-machine systems. *Int. J. Electr. Power Energy Syst.* **2014**, *63*, 132–139. [CrossRef]

Disclaimer/Publisher's Note: The statements, opinions and data contained in all publications are solely those of the individual author(s) and contributor(s) and not of MDPI and/or the editor(s). MDPI and/or the editor(s) disclaim responsibility for any injury to people or property resulting from any ideas, methods, instructions or products referred to in the content.